Er-Doped Integrated Optical Devices in LiNbO$_3$

I. Baumann, S. Bosso, R. Brinkmann, R. Corsini, M. Dinand, A. Greiner,
K. Schäfer, J. Söchtig, W. Sohler, H. Suche, and R. Wessel

(Invited Paper)

Abstract— **The state-of-the-art of Er-doped integrated optical devices in LiNbO$_3$ is reviewed starting with a brief discussion of the technology of Er-indiffusion. This technique yields high-quality waveguides and allows a selective surface doping necessary to develop optical circuits of higher complexity. Doped waveguides have been used as single- and double-pass optical amplifiers for the wavelength range 1530 nm $< \lambda <$ 1610 nm. If incorporated in conventional, lossy devices loss-compensating or even amplifying devices can be fabricated. Examples are an electrooptically scanned Ti:Er:LiNbO$_3$ waveguide resonator used as an optical spectrum analyzer and an acoustooptically tunable filter used as a tunable narrowband amplifier. Different types of Ti:Er:LiNbO$_3$ waveguide lasers are presented. Among them are free running Fabry–Perot lasers for six different wavelengths with a conitnuous-wave (CW)-output power up to 63 mW. Tunable lasers could be demonstrated by the intracavity integration of an acoustooptical amplifying wavelength filter yielding a tuning range up to 31 nm. With intracavity electrooptic phase modulation modelocked laser operation has been obtained with pulse repetition frequencies up to 10 GHz; pulses of only a few ps width could be generated. With intracavity amplitude modulation Q-switched laser operation has been achieved leading to the emission of pulses of up to 2.4 W peak power (0.18 μJ) at 2 kHz repetition frequency. Distributed Bragg reflector (DBR) lasers of emission linewidth $\leq$8 kHz have been developed using a dry-etched surface grating as one of the mirrors of the laser resonator. Finally, as an example for a monolithic integration of lasers and extracavity devices on the same substrate, a DBR-laser/modulator combination is presented.**

I. INTRODUCTION

DURING the last few years, there has been a growing interest in rare-earth doped optically pumped amplifier and laser devices in LiNbO$_3$ [1]–[7]. In particular, Er-doped devices operating in the third telecommunication window around 1.55-μm wavelength have attracted much attention [8]. The combination of the amplifying properties of the dopant erbium with the excellent electrooptical and acoustooptical properties of the waveguide substrate LiNbO$_3$ allows the development of a whole class of new waveguide devices of higher functionality. Loss compensated or even amplifying

devices have been fabricated by doping the corresponding waveguide structures [9], [10]. Very simple, but efficient waveguide lasers have been developed [11]. By intracavity integration of modulators and wavelength filters modelocked [12], [13], Q-switched and tunable lasers [14] have been realized. Moreover, the different types of lasers and amplifiers can be combined with other active and passive devices on the same substrate [15] to form integrated optical circuits (IOC's) for a variety of applications in optical communications, sensing, signal processing and measurement techniques.

It is the aim of this paper to review the state-of-the-art of Er-doped integrated optical devices in LiNbO$_3$; most of them have been developed in the EDIOLL-project (erbium-doped integrated optical lithium niobate lasers) of the RACE II-program of the European Union.

In Section II, the technology of fabricating Er-diffusion doped waveguides in LiNbO$_3$ substrates is briefly discussed. If optically pumped such doped waveguides can be used as optical amplifiers (Section III). Examples of loss-compensated and amplifying devices are given in Section IV. In Section V, the different types of lasers demonstrated up to now are presented. A laser/modulator transmitter unit is described in Section VI as an attractive example of a monolithically integrated optical circuit in LiNbO$_3$. Finally, the paper is finished with some concluding remarks.

II. Er-DIFFUSION DOPED WAVEGUIDES

In principle, there are two ways to fabricate Er-doped waveguides in LiNbO$_3$: homogeneously-doped or surface-doped crystalline wafers can be used as waveguide substrate. Homogeneous doping can be achieved during crystal growth from an Er-doped melt [16]. However, it is difficult to achieve high-quality striation-free crystals of high doping concentration and large size. The introduction of rare earth ions tends to increase the number of domains in the crystal [17]. On the other hand, Er-doping of a surface layer as alternative can be achieved by implantation and annealing [18] or by indiffusion of vacuum-deposited Er-layers [19], [20]. For these techniques commercially available LiNbO$_3$-wafers of high optical quality and large diameter can be used. The latter method is easy to apply and ideally suited for a selective doping of the surface using photolithographic patterning of the evaporated Er- or Er$_2$O$_3$-layers, respectively. Selective doping is a prerequisite for the monolithic integration of active (optically pumped, Er-doped) and passive (unpumped) devices on the same substrate to avoid reabsorption in unpumped Er-doped waveguides.
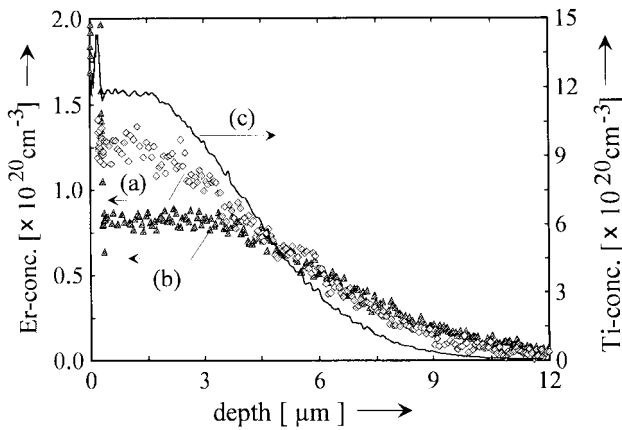
Fig. 1. Erbium and titanium concentrations versus depth in a $\hat{Z}$-cut LiNbO$_3$ wafer measured by SNMS. (a) Er-profile after indiffusion of a 22-nm-thick Er-layer at 1130 °C within 100 h. (b) Er-profile after additional indiffusion of a 95-nm-thick Ti-layer at 1030 °C within 9 h. (c) Corresponding Ti-distribution.

The process of Er-indiffusion has been characterized in detail using secondary ion mass spectroscopy (SIMS), secondary neutral mass spectroscopy (SNMS), Rutherford backscattering spectroscopy (RBS), and atomic force microscopy (AFM) [21]. The site of the Er^{3+}-ions in the LiNbO$_3$-lattice has been determined using X-ray standing wave spectroscopy (XSW) [22] and optical site selective spectroscopy (OSSS) [23].

The diffusion of erbium into LiNbO$_3$ can be described by Fick's laws with a concentration-independent diffusion coefficient and a temperature-dependent maximum solubility [21]. Typical Er-doping profiles before and after the fabrication of a planar Ti-indiffused waveguide in a $\hat{Z}$-cut LiNbO$_3$ substrate are shown in Fig. 1 together with the Ti-profile. Due to the anisotropic crystal structure of LiNbO$_3$ the diffusion coefficient of Er in LiNbO$_3$ depends on the crystal cut with the highest diffusivity along the crystal $\hat{Z}$-axis. This can be clearly seen in Fig. 2 where the temperature dependent diffusion coefficients derived from measured Er-concentration profiles have been plotted as Arrhenius-diagrams [21]. From the slope and the offset of the graphs the cut-dependent diffusion constants D$_0$ and activation energies E$_a$ have been determined, respectively. The diffusion coefficients are about two orders of magnitude smaller than those of titanium. Therefore, the Er-diffusion-doping has to be performed prior to the waveguide fabrication. To achieve a good overlap of doping profile and the optical waveguide modes the Er-diffusion has to be performed at a temperature as high as possible and close to the Curie-temperature of ferroelectric LiNbO$_3$ (1142 °C for congruent melting material [24]) for at least 100 h (see also Fig. 1). The solubility of erbium (about 1.7×10^{20} cm^{-3} at 1100 °C) is about one order of magnitude smaller than that of titanium; it grows exponentially with the temperature [21].

During indiffusion of a vacuum-deposited Er-layer the surface concentration of the dopant corresponds to the solubility level as long as the diffusion reservoir is not exhausted. Afterwards, the concentration drops according to Fick's laws. To prevent the formation of precipitates of Er$_x$Nb$_y$-oxide compounds during the waveguide fabrication the Er-surface concentration should be at least slightly below the solid solubility level at the waveguide fabrication temperature.
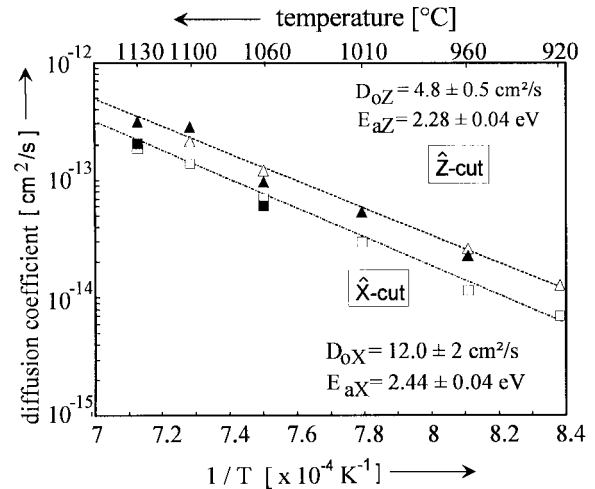

Fig. 2. Arrhenius plots of the diffusion coefficients of erbium into LiNbO$_3$ for diffusion parallel to the c-axis - $\hat{Z}$-cut - (triangles) and perpendicular to the c-axis - $\hat{X}$-cut - (squares) of the LiNbO$_3$-crystal derived from the concentration profiles determined by SIMS- (white) and SNMS- (black) measurements.

Er is incorporated into LiNbO$_3$ on a vacant Li-site or replaces lithium [22]. The exact position compared with the Li-site is shifted by 0.46 Å in ($-c$)-direction. Absorption measurements and site-selective spectroscopy found four slightly different erbium sites [23]. This has been attributed to perturbations of the local crystal field due to variations of the arrangement of charge compensating defects.

Up to now, Er-doped waveguides of very low scattering losses could only be fabricated by Ti-indiffusion into the Er-doped LiNbO$_3$-surface; the proton-exchange technique gave waveguides of lower quality. The fluorescence yield of the $^4I_{13/2} \rightarrow {}^4I_{15/2}$—transition is very low and the scattering losses of Er-diffusion doped annealed and proton exchanged LiNbO$_3$-waveguides could not be reduced below $\simeq 1$ dB/cm [38]. To be specific, scattering losses below 0.1 dB/cm have been measured in doped Ti-diffused waveguides with an Er-surface concentration up to $\simeq 5 \times 10^{19}$ cm^{-3}.

III. WAVEGUIDE AMPLIFIERS

An Er-doped Ti:LiNbO$_3$-channel waveguide—if optically pumped—can be used as an optical amplifier in the wavelength range 1.53 μm $< \lambda <$ 1.62 μm. Amplification has been intensively investigated for different Er-doping levels and in two different configurations: single-pass and double-pass [25]. In the latter case, a highly reflecting broadband mirror has been deposited on the rear endface of the waveguide to double the interaction length of pump and signal modes. In this way the pump absorption efficiency is improved and the signal gain is increased.

To excite the Er-ions radiation of $\lambda_p \simeq 1480$ nm has been used, which has several advantages compared to pumping at $\simeq 980$-nm wavelength (the prefered pump wavelength for Er-doped fibers): Ti-diffused waveguides in LiNbO$_3$, which are fabricated to be single mode in the wavelength range 1530 nm$\leq \lambda \leq$ 1620 nm are multimode at 980 nm. Therefore, by pumping at 1480 nm the problem of selective mode excitation
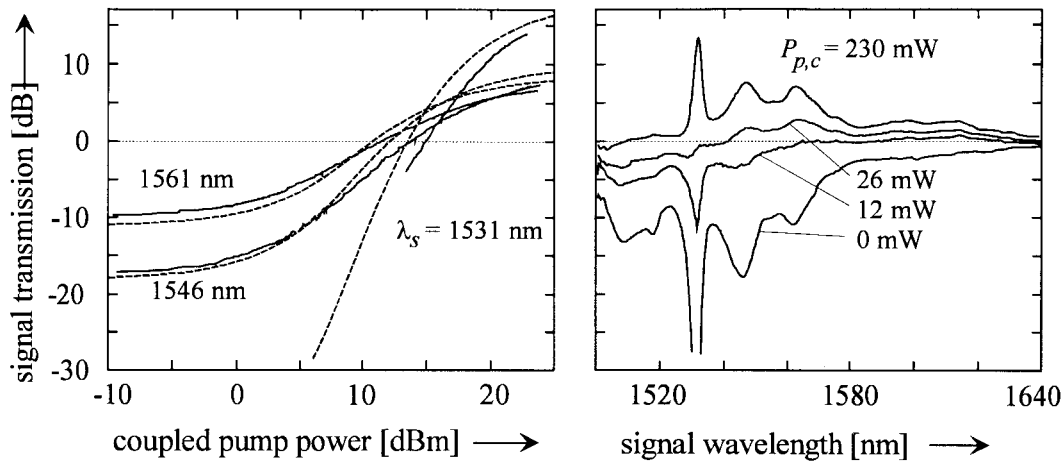
Fig. 3. Signal transmission (net absorption/gain) of a 70-mm-long optically pumped Ti:Er:LiNbO$_3$ ($\hat{Z}$-cut) waveguide amplifier versus signal wavelength at different levels of coupled pump power (right) and versus coupled pump power ($\lambda_p = 1480$ nm) at the signal wavelengths of gain maxima. Doping and waveguide fabrication correspond to the data of Fig. 1. Both, signal and pump polarization are TE (σ). Solid lines: experimental, dashed lines: calculated data.
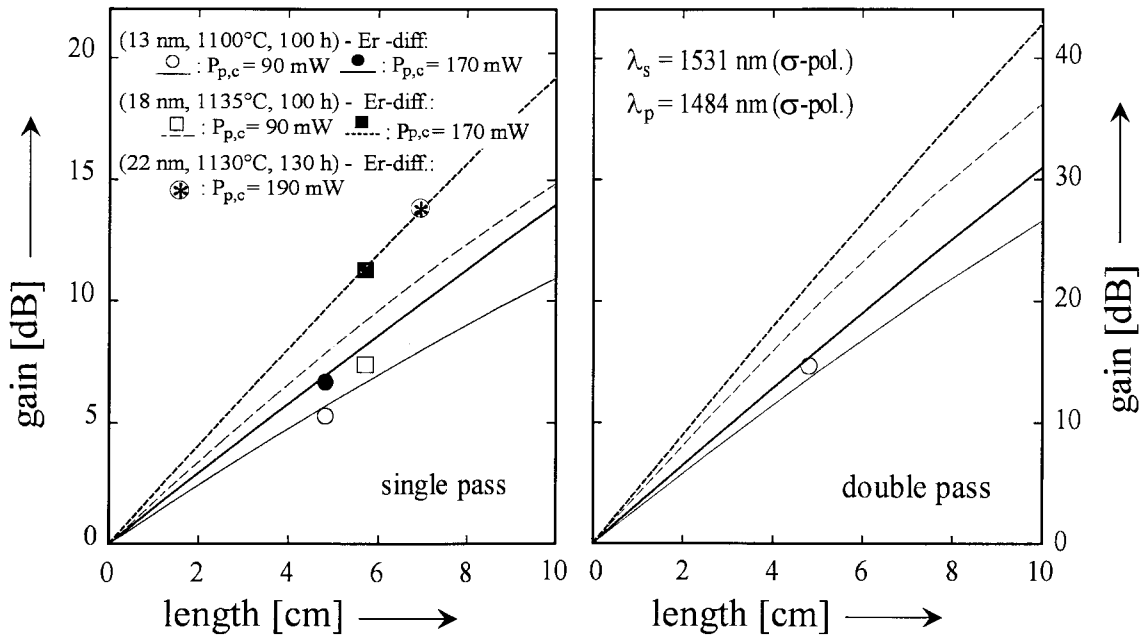

Fig. 4. Calculated (lines) and measured (marks) gain versus length of Ti:Er:LiNbO$_3$-waveguide amplifiers for single-pass (left) and double-pass configurations (right). Thickness of indiffused Er-layers, diffusion temperatures, diffusion time and coupled pump-power levels are given as inset.

can be avoided. As the mode sizes of pump and signal are almost identical, a perfect overlap is guaranteed. Moreover, up-conversion leading to visible fluorescence and photorefraction effects are much weaker for 1480-nm pumping than for 980-nm pumping.

Results of the pump power dependent signal transmission of a 7-cm-long single-pass amplifier are shown in Fig. 3 as an example [25]. The investigated waveguide has been fabricated by indiffusion at 1030 °C for 9 h of a 6-μm-wide, 95-nm-thick Ti-stripe into a 7-cm-long $\hat{Z}$-cut LiNbO$_3$-substrate Er-doped near the surface by indiffusion of a 22-nm-thick evaporated Er-layer at 1130 °C during 100 h. Both pump- and signal polarization have been adjusted perpendicular (σ) to the crystal c-axis exciting TE-modes in the waveguide. The right diagram gives the transmission spectra for different levels

of the coupled pump power. The lowest graph corresponds to the absorption spectrum of Er:LiNbO$_3$. With increasing pump power the absorption is bleached and gradually converted into gain, first at longer wavelengths. At the highest pump power, the maximum gain peak of 13.8 dB is at 1531-nm wavelength. In the diagram on the left, the measured (solid lines) and calculated dependence (dotted lines) of three gain maxima on the coupled pump power is plotted. It should be emphasized that the length of the amplifying waveguide is far below the optimum length of full pump exploitation. To illustrate the potential for further improvements, Fig. 4 presents the predicted net gain versus waveguide length (lines) together with selected experimental results (marks) for single- (left) and double-pass amplifiers (right). With a double-pass device fabricated in a commercially available LiNbO$_3$-wafer
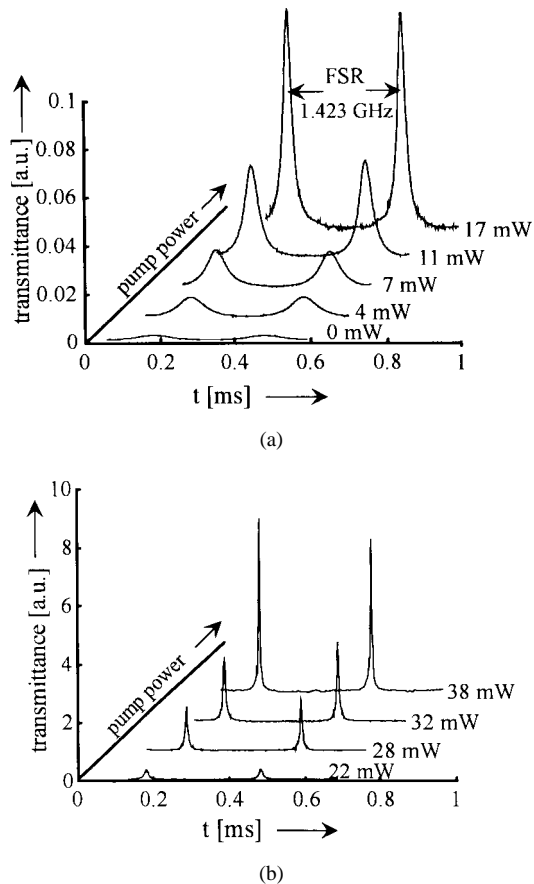
Fig. 5. Transmittance of an electrooptically scanned Ti:Er:LiNbO₃ waveguide resonator versus time with the coupled pump power as parameter. The sawtooth drive voltage changes by V_π within $\simeq 300$ μs corresponding to one free spectral range FSR = 1.423 GHz of the cavity.
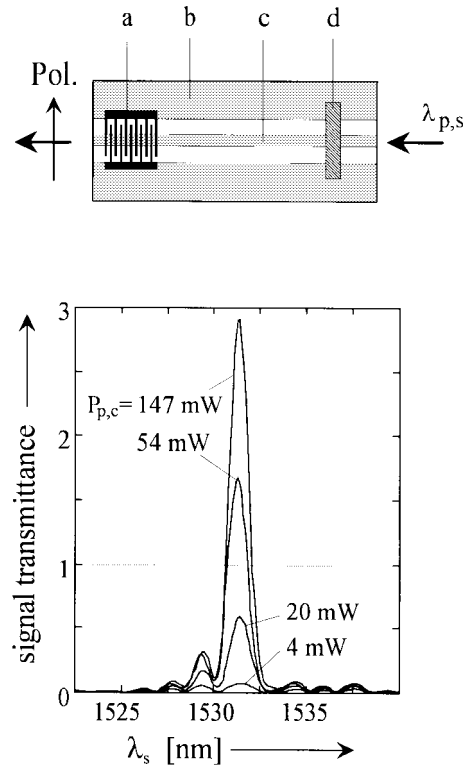

Fig. 6. Upper part: Scheme of the amplifying single stage Ti:Er:LiNbO₃ mode-converter with external polarizer (Pol.). (a) interdigital transducer; (b) Ti-diffused claddings of the acoustic waveguide; (c) Ti-diffused optical waveguide; (d) acoustic absorber. Lower part: transmittance of the filter versus wavelength for different levels of coupled pump power; incident signal and pump polarization: σ (TM); pump wavelength: 1484 nm; acoustic frequency: 174.94 MHz; RF-drive power: 17 dBm.

of 4-in diameter net gain up to 40 dB seems to be possible; however, upconversion effects, which could reduce the amplifier efficiency at high-signal levels, have not been taken into account in the calculations.

IV. LOSS COMPENSATED AND AMPLIFYING DEVICES

In LiNbO₃ a variety of passive and active devices of excellent performance, e.g., filters, modulators and switches, have been developed in the past for which coupling and internal loss (over-)compensation would be highly desirable ("0 dB- and amplifying devices"). Er-doping can be an attractive means to provide the necessary gain by optical pumping. In the following, two specific examples of such devices are presented.

A. Loss Compensated Electrooptical Spectrum Analyzer

Finesse enhancement in waveguide cavities by internal gain has been first demonstrated in Er-doped fiber- and silica-based integrated optical ring cavities [26], [27]. However, these materials only allow a slow thermooptical or mechanical scanning of the cavity resonances. For fast spectral analysis an electrooptically tunable Ti:LiNbO₃-waveguide cavity is attractive as integrated optical spectrum analyzer (IOSA); the scanning speed is only limited by the finite cavity build-up time. We

have utilized an Er-diffusion-doped intracavity amplifier for loss compensation leading to finesse enhancement and in this way to a strong increase of the spectral resolution [9]. The 48 mm long device is an Er-doped Ti:LiNbO₃-waveguide resonator with monolithically integrated phase modulator and dielectric mirrors on both end faces. It has been fabricated in $\hat{X}$-cut LiNbO₃ doped near the surface by indiffusion of a 9.2-nm-thick erbium layer at 1100 °C during 100 h. The cavity mirrors have been deposited using ion-beam-assisted evaporation of SiO₂–TiO₂ layers. To allow endfire pumping of the active IOSA, the pump coupler has been made dichroitic with a high transmittance at the pump wavelength (T $\simeq$ 0.65 at λ_p = 1479 nm) and simultaneously a high reflectance (R$\simeq$0.97) at 1546 nm, the wavelength of the investigated signal source (distributed feedback (DFB) laser diode). The output coupler has a reflectance of about 0.98 at both, pump and signal wavelengths, allowing a double-pass of the pump in the cavity. The active IOSA has been diode-pumped at λ_p = 1479 nm (E$_p\|$ c) as close as possible to its lasing threshold. Linear scanning of the cavity resonances has been achieved by driving the intracavity electrooptic phase modulator (U$_\pi$ $\simeq$10.4 V) with a sawtooth voltage. The results of such a measurement are shown in Fig. 5. The transmitted spectral power density of the investigated signal source (DFB-laser) is plotted versus time. The change of the sawtooth drive voltage by V_π within $\simeq$300 μs corresponds to one free spectral
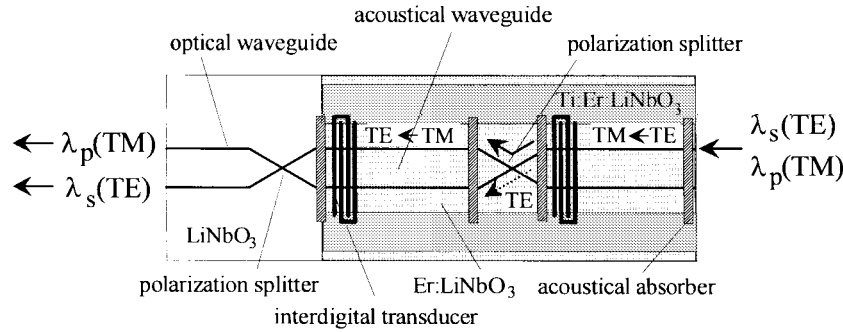
Fig. 7. Schematical sketch of an amplifying, double-stage acoustooptical wavelength filter with integrated polarizers (polarization splitters) for polarization-dependent (see diagram) or -independent operation (see text). The routing of the converted and unconverted signal light is indicated for polarization dependent operation.

range FSR = 1.423 GHz of the cavity. Parameter of the set of graphs is the launched pump power. A finesse up to 205 has been achieved corresponding to a spectral resolution of about 6.9 MHz, which allowed to measure the spectral width (16 MHz) of the DFB-laser diode investigated. This improved resolution is accompanied by an increase of the cavity transmittance by three orders of magnitude. In this way the spectral investigation of low power sources is facilitated.

B. Amplifying Acoustooptically Tunable Wavelength Filter

Acoustooptically tunable wavelength filters are very attractive devices for wavelength division multiplex applications in optical communications due to their unique multi-wavelength filtering capability [28]. However, filters of low crosstalk require double-stage conversion concepts [29] inducing increased insertion losses. Therefore, loss compensation or even overall gain is desirable.

As a first step toward a fully integrated, amplifying, double-stage filter a single stage acoustooptically tunable TE-TM-mode converter has been fabricated in an Er-doped LiNbO₃-substrate. In combination with an external polarizer tunable filtering over a wavelength range of 70 nm accompanied by amplification has been demonstrated [10]. The structure of the mode converter is shown together with the filter response at different pump power levels in Fig. 6. The device has been fabricated in an Er-diffusion-doped $\hat{X}$-cut LiNbO₃-substrate. It consists of a combined acoustical and optical waveguide structure, which is defined by Ti-indiffused regions forming the claddings of the acoustic waveguide of 100-μm width (b) and by a 7-μm-wide Ti-diffused stripe forming the core of the optical channel guide (c). The interdigital transducer (a) for the excitation of the guided surface acoustic wave (SAW) has been photolithographically defined. An acoustic absorber (d) terminates the interaction length of SAW and optical modes.

To investigate the performance of the device, a fiber-pigtailed luminescence diode has been used as signal source and a tunable color center laser (CCL) as the pump. The input polarization of both, signal and pump, have been adjusted to TM (σ). To block the nonpolarization-converted signal at the output an external polarizer has been used. The signal was then fed into a monochromator of 0.5 nm resolution for spectral analysis.

On the lower part of Fig. 6, the signal transmission through the acoustooptical filter is shown versus wavelength for different levels of coupled pump power (λ_p = 1484 nm). The acoustic frequency, which determines the wavelength of phase-matched acoustooptic mode conversion (here λ_s = 1531 nm), was 174.94 MHz; the RF-power level has been adjusted for complete conversion. At coupled pump power levels higher than about 30 mW the signal transmission is larger than unity. In this case the filter acts as a narrow band tunable amplifier. A maximum amplification of 4.8 dB with a coupled pump power of 22 dBm ($\simeq$160 mW) has been obtained at λ_s = 1531 nm. With a coupled pump-power level of 140 mW the gain is higher than 1.6 dB in the whole wavelength band 1540 nm < λ_s < 1565 nm with maxima of 2.9 dB at 1546 nm and 2.6 dB at 1561 nm. If a flat gain is required, the transmission of the device can be adjusted by appropriate levels of the driving RF-power.

These results are encouraging. However, the narrow-band amplifier has a poor sidelobe suppression of the filter characteristics, the frequency of the converted wave is shifted by the acoustic frequency, the required polarizer is not integrated and the device does not operate polarization-independent. Therefore, a fully integrated version of a doped double-stage filter with integrated polarization splitters and a second frequency shift compensating mode converter has been realized; it can be operated as a polarization-dependent or (nearly) polarization-independent, amplifying filter.

The structure of this more advanced device is shown schematically in Fig. 7. The polarization-dependent routing is indicated for both TE-polarized signal and TM-polarized pump superimposed in the upper right branch of the optical waveguide structure (polarization-dependent operation). Only the phase-matched part of the signal is converted by the first acoustooptical mode converter to TM and passes—together with the pump mode—the right polarization splitter in the bar state. The unconverted part of the TE-polarized signal is directed cross to the unpumped lower branch of the left mode converter and hence absorbed. The already once-filtered TM-polarized signal light is converted again to TE in the left- (second-) mode converter and routed by the second-polarization splitter, which separates the pump, to the lower left output.

If polarization-independent operation is required, both arms of the left mode converter have to be pumped. This can be achieved by a simultaneous excitation of TE- and TM-pump modes of nearly equal amplitude at the input of the filter. However, due to the splitting of the pump power, the overall filter gain is reduced in comparison with the polarization-dependent operation.

The advanced filter structure has increased losses due to the additional optical and acoustical components. The second transducer induces an excess loss of 0.2 dB, each of the polarization splitters of about 0.7 dB for TE- and TM-modes. Nevertheless, up to about 1-dB net signal gain has been measured at 1546 nm in the polarization-dependent mode of operation. Therefore, the filter can also be used as intracavity tuning element in a Fabry–Perot waveguide laser (see Section V-B).

V. WAVEGUIDE LASERS

Waveguide amplifiers are the basic devices to develop integrated lasers. Incorporated in an optical cavity to achieve the necessary feedback laser oscillation can be obtained by sufficient optical pumping exceeding the threshold level. The simplest laser is a free running (without intracavity control devices) Fabry–Perot laser. It has the lowest intracavity losses, and therefore, the potential for a high-power conversion efficiency. Such a device of optimized efficiency will be presented in Section V-A. More advanced lasers can be developed by integrating a modulator or (and) a wavelength filter in the waveguide resonator. In this way, an amplifying acoustooptical filter—as discussed before—leads to tunable laser operation; a corresponding device is presented in Section V-B. An intracavity phase- or amplitude modulator allows to obtain modelocked operation and therefore the generation of ultrashort pulses. This is discussed in Section V-C. Moreover, the intracavity amplitude modulator offers the posibility for Q-switched operation of the laser and in this way for the generation of short pulses of high power. Such a Q-switched laser is presented in Section V-D. All these different types of lasers have dielectric cavity mirrors, deposited on the polished waveguide endfaces. The rear mirror (which is the output coupler) has a high reflectivity not only at the signal but also at the pump wavelength to provide double-pass pumping and in this way an improved pump absorption efficiency.

One (or even both, in the future) of the dielectric mirrors can be replaced by a Bragg-grating, etched into the surface of the waveguide amplifier. Its narrow-band reflectivity precisely determines the wavelength of the laser emission. Moreover, such a DBR laser, which is described in Section V-E, facilitates the monolithic integration of the laser with further devices on the same substrate.

A. Free-Running Fabry–Perot Lasers

In a Fabry–Perot-type laser without any wavelength-controlling intracavity device the emission wavelength is determined by the spectral properties of the cavity (wavelength-dependent mirror reflectivities, amplifier gain spectrum and waveguide scattering losses) and, therefore, by

the pump power level as well. By a proper choice of the output coupler laser emission at the different maxima of the Er:LiNbO$_3$-gain spectrum can be achieved. Up to now, lasers of six different wavelengths have been fabricated: $\lambda_s = 1531$, 1546, 1562, 1576, 1602, and 1611 nm [11]–[13], [30], [31]. However, it is a problem to design the cavity in such a way that maximum quantum efficiency is obtained. In any case, the waveguide amplifier should have low-scattering losses and a high-absorption efficiency; both can be achieved by an optimized Er-doping profile, an optimized waveguide length and a double-pass pumping scheme. All the waveguide and amplifier parameters then determine the optimum output coupler. Following these guidelines, a laser of optimized efficiency has been recently demonstrated [11]. It has a heavily Er-doped straight Ti-diffused channel guide of 7-cm length with a small-signal gain of up to 13.8 dB achieved with a coupled pump power of 190 mW (see Section III). Using numerical simulations based on the theoretical model for Er-doped waveguide amplifiers [32], the optimum output coupler was determined to have a maximum reflectivity of 30 % at $\lambda_s = 1562$ nm corresponding to a 70% output coupling efficiency. This mirror guarantees that laser oscillation sets in at $\lambda_s = 1562$ nm with highest quantum efficiency. A maximum output power of 63 mW at an incident pump-power level of 210 mW (CCL-pumping) has been obtained (see Fig. 8). The lasing threshold was only 24 mW. A slope efficiency up to 37% has been observed. These experimental results are in good agreement with the theoretical predictions. The waveguide laser has been pigtailed, packaged and characterized again using diode-pumping at about 1480-nm wavelength; the result is shown in the lower graph of Fig. 8. Only a slight increase of the threshold and a slight decrease of the output power was caused by the pigtailing. A maximum output power of 14 mW with strongly reduced noise was achieved at a pump power level of 95 mW. Moreover, spectral noise measurements showed that at frequencies above 50 MHz, the laser output is shot noise limited, while at low frequencies around 350-kHz residual relaxation oscillations are observed. They can be drastically suppressed by a feedback controlled pumping (see Section V-C).

A further improvement of the laser efficiency seems to be possible. Theoretical calculations predict, that a reduction of the scattering losses from 0.18 dB/cm (actual sample) down to 0.08 dB/cm would increase the maximum slope efficiency by more than 10% [11]. A higher Er-doping level and improved overlap of the doping profile and the waveguide modes would increase the output power further.

B. Acoustooptically Tunable Laser

Since the first demonstration of an acoustooptically tunable Ti:Er:LiNbO$_3$-waveguide laser in 1994 [14], a significant improvement of its performance has been achieved as a result of a better design with reduced intracavity losses. The design is based on the double-stage wavelength filter with polarization-dependent operation presented in Section IV-B. The main difference to the old design described in [14] is the replacement of the TE-pass polarizer by a more stable
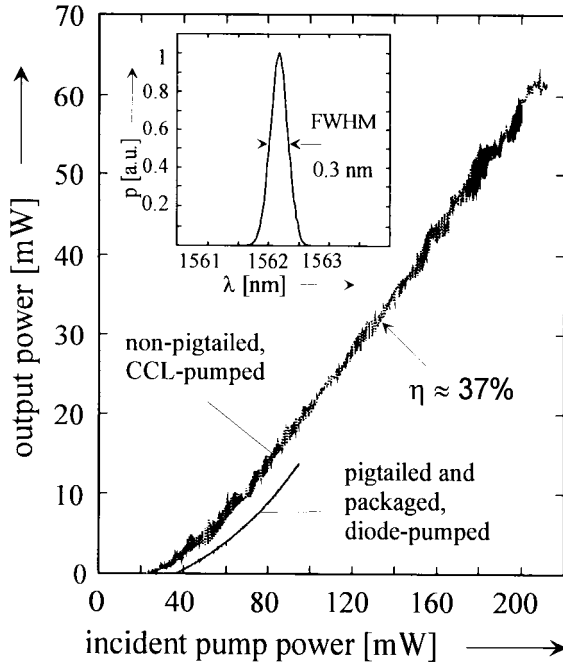
Fig. 8. Output power of a laser diode pumped, pigtailed and packaged Ti:Er:LiNbO$_3$ waveguide laser of optimized efficiency versus incident pump power. Both, pump and signal polarization are TE (σ). For comparison the power characteristics of the color center laser- (CCL-) pumped waveguide laser without pigtails is given. Inset: emission spectrum of the diode pumped (95 mW) waveguide laser.

Fig. 9. Emission wavelength versus acoustic frequency of pigtailed, packaged and diode pumped acoustooptically tunable Ti:Er:LiNbO$_3$-waveguide laser for 127 mW of incident pump power. Inset: power characteristics of the laser for selected wavelengths.

and less lossy polarization splitter. Moreover, the Er-doping and waveguide fabrication have been optimized to give a better pump absorption efficiency, higher signal gain and lower scattering losses. The bandwidth of the filter of 1.35 nm (FWHM) resulted in a laser emission linewidth of about 0.25 nm. One of the two integrated intracavity polarization splitters is utilized as pump-coupler thus allowing the use of a simple Au-mirror as the rear cavity reflector. The output coupler of the 63-mm-long laser cavity is a dielectric mirror of about 98 % reflectance. Reduced scattering losses of the waveguides—0.1 dB/cm for TE-polarized light and 0.05 dB/cm for TM-polarization—and low insertion losses of the other intracavity components resulted in a total cavity round trip loss of $\simeq$ 4.8 dB.

The laser has been fiber-pigtailed, packaged and characterized using diode pumping (λ_p = 1484 nm). The minimum threshold of the packaged device was about 50 mW at $\lambda_s \approx$ 1561 nm (see power characteristics as an inset in Fig. 9). With about 110 mW coupled pump power in TE-polarization up to 320-μW TM-polarized output power has been measured. The nonlinearity of the power characteristics is attributed to a change of the spectrum of the pump laser diode during the sweep of the injection current. The overall tuning behavior for diode pumping of the packaged device is shown in Fig. 9. The tuning slope is −8 nm/MHz. In the gaps of the tuning characteristics, the internal gain was not sufficient to overcome the round trip losses in the laser cavity. However, by using a color center laser as pump source of higher power level continuous tuning from 1540 to 1568 nm was possible. By optical isolation of the laser, output and feedback controlled pumping
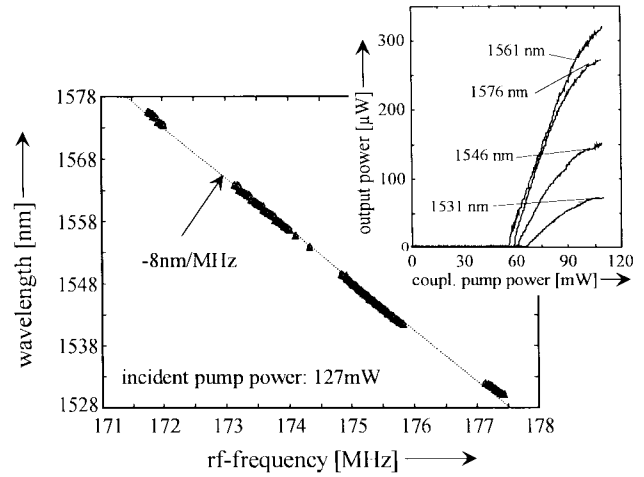
fairly stable laser operation with a RIN below −125 dB/Hz for frequencies above 50 MHz has been achieved at an output power level of 108 μW.

C. Modelocked Lasers

Up to now modelocked laser operation of Ti:Er:LiNbO$_3$ waveguide lasers has been achieved by intracavity phase modulation synchronously with the fundamental [12] or with harmonics [13] of the axial mode frequency spacing of the laser cavity. Modelocking has been demonstrated with lasers in both, $\hat{X}$- and $\hat{Z}$-cut LiNbO$_3$ substrates. Devices in $\hat{Z}$-cut material profit from the slightly lower waveguide attenuation and a higher gain but require an insulating buffer-layer under the electrodes of the phase modulator to prevent excess absorption losses. The design of such a laser in $\hat{Z}$-cut LiNbO$_3$ is schematically shown in the upper part of Fig. 10. To allow efficient phase modulation at different harmonics of the axial mode frequency spacing a broadband traveling-wave modulator has been used with thick electroplated Au-electrodes (details of the fabrication of the waveguide and the laser cavity can be found in [13]). Via the largest electrooptic coefficient the extraordinary index of refraction is modulated leading to the coupling of the longitudinal TM-modes of the laser. It is pumped by a pigtailed laser diode in TM-polarization ($\lambda_p \simeq$1480 nm). The modelocked Ti:Er:LiNbO$_3$ waveguide laser has been characterized in terms of power characteristics, time–bandwidth product of the output pulses and detuning behavior. Threshold figures as low as 9 mW at λ = 1602 nm and an average output power of 1.1 mW (at 75-mW pump power) have been achieved. To determine the width of the pulses in the time- and frequency-domain an optical autocorrelator and a spectrometer of about 0.1-nm spectral resolution have been used. Driven by the fundamental round-trip frequency of 1.281 GHz of the 5.4-cm-long laser resonator with a RF-drive power of 31.5 dBm pulses of 8.6 ps FWHM and 650-mW peak power were observed. With harmonic modelocking, the pulse width could
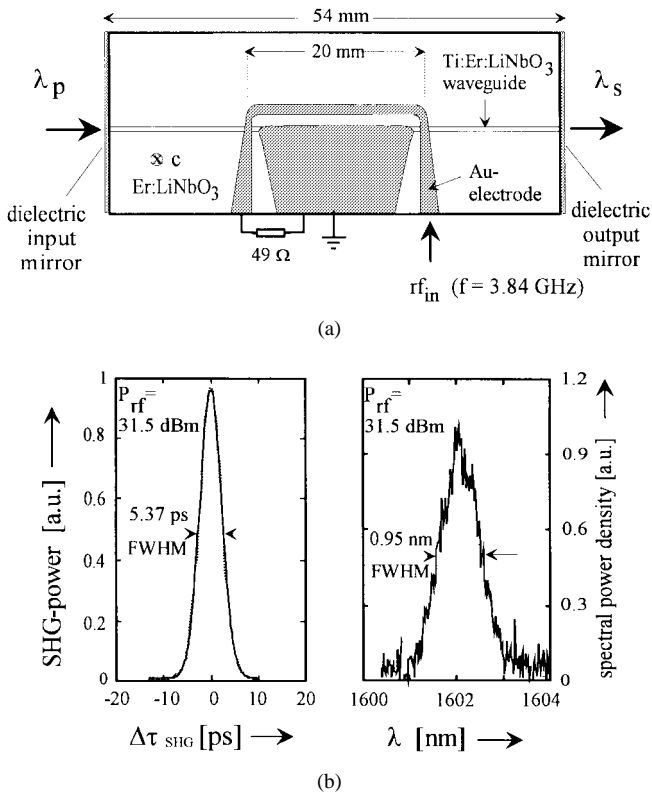
(a)

(b)

Fig. 10. Upper part: structure (schematical) of an FM-modelocked Ti:Er:LiNbO$_3$-waveguide laser with 20-mm-long traveling-wave phase modulator as modelocker. Lower part: autocorrelation trace (left) and optical spectrum (right) for third-harmonic modelocking.

be further reduced. As an example, at the third-harmonic (3.843-GHz) pulses of 3.8-ps FWHM and 63-mW peak power could be generated at the same RF-drive power level. In the lower part of Fig. 10, an autocorrelation trace and the optical spectrum of the laser emission for third-harmonic modelocking are shown. From the FWHM of both graphs (and after deconvolution of the correlation trace measured by second harmonic generation), a time–bandwidth product of $\simeq$ 0.42 can be determined. This figure agrees very well with the time-bandwidth-product of transform limited Gaussian pulses. According to the theory of Kuizenga and Siegman [33] such transform limited pulses require for FM-modelocking a slight negative detuning of the modelock frequency from the fundamental, respectively, harmonics of the axial mode frequency spacing. Harmonic modelocking has been observed up to the 8th harmonic (10.24-GHz pulse repetition frequency), limited only by present RF-signal generator.

Relaxation oscillations can seriously degrade the amplitude stability of the modelocked pulses. However, this issue can be almost eliminated by feedback controlled pumping of the Er-laser. For that purpose a fraction of the modelocked laser output is detected. The deviation of the detector current from an average figure (corresponding to the time-averaged output of the modelocked laser) is utilized as an error signal to control the injection current of the pump laser diode. In Fig. 11, the relative intensity noise of the FM-modelocked laser of 1.28-GHz pulse repetition frequency (fundamental modelocking) is shown for controlled and uncontrolled pump-
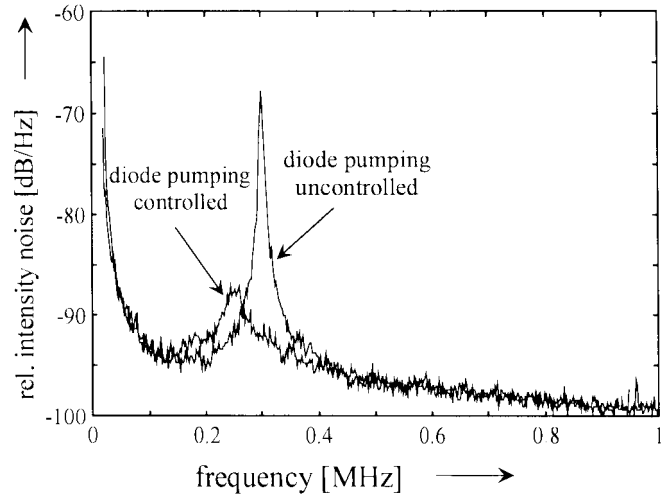

Fig. 11. Relative intensity noise (RIN) versus frequency of the diode-pumped FM-modelocked Ti:Er:LiNbO$_3$ waveguide laser with and without feedback controlled pumping.

ing, respectively. With uncontrolled pumping (constant current injection), the peak of the noise spectrum at the relaxation oscillation frequency ($\simeq$ 280 kHz at the chosen pumping level) is very pronounced. With controlled pumping the peak is suppressed by about 20 dB and slightly shifted to lower frequencies.

D. Q-Switched Laser

Very recently, a Ti:Er:LiNbO$_3$ waveguide laser with intra-cavity Er-doped Mach–Zehnder-type intensity modulator has been developed. It has a dielectric mirror of 98% reflectivity at both, pump ($\lambda_p \simeq 1480$ nm) and laser emission wavelengths ($\lambda_s \simeq 1561$ nm) on one side of the waveguide resonator. On the other side a variable output/pump coupler mirror has been realized by an adjustable, piezoelectrically driven air gap etalon formed by the endfaces of the pump input/signal output fiber and the polished Ti:Er:LiNbO$_3$-waveguide endface. With diode pumping a threshold of about 58 mW has been achieved.

The intracavity modulator allows to control the cavity loss, which is the basis for Q-switched laser operation to generate pulses of high peak power. At large cavity losses (low-Q) the pump drives, the population inversion of the involved Er^{3+}-energy states up to a saturation level, which is determined by the onset of prelasing due to the residual cavity finesse. The better the modulator extinction is the more the stored energy in the laser active ions grows before prelasing sets in. After switching to low cavity losses (high-Q) the population inversion is rapidly reduced by the emission of a pulse of high peak power.

In Fig. 12, first results of Q-switched operation of the Ti:Er:LiNbO$_3$ laser, just desribed, are presented. The laser is continously pumped with 100 mW. After switching to the high-Q cavity, which corresponds to the zero of the abszissa, pulses of a peak power up to 2.4 W and a pulse energy of 0.18 μJ are emitted at 2-kHz repetition frequency. With increasing frequency the pulses become broader, the peak power is reduced and the pulse build-up-time increases.
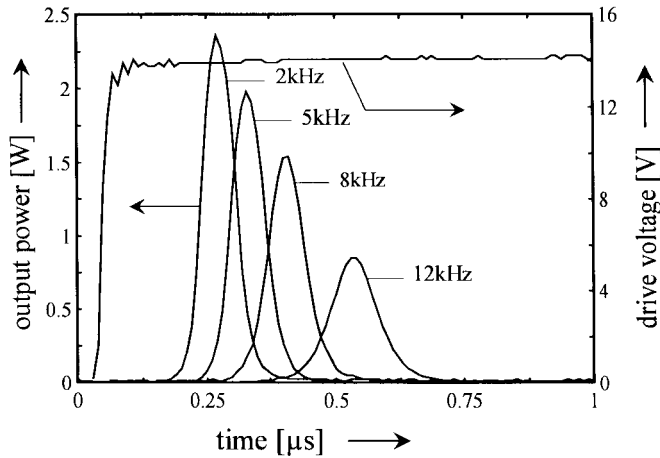
Fig. 12. Output power (left ordinate) and drive signal of the intracavity amplitude modulator (right ordinate) of a Q-switched Ti:Er:LiNbO$_3$ waveguide laser versus time. Parameter is the pulse- or Q-switching repetition frequency.

E. Narrow Linewidth DBR-Laser

By replacing one of the dielectric endface mirrors of a Fabry–Perot type laser by a (first-order) Bragg-grating etched into the surface of Ti:Er:LiNbO$_3$ channel guides distributed Bragg reflector (DBR) lasers have been fabricated. Their emission wavelength is determined by the periodicity of the grating. Even single frequency operation can be expected in case of a grating response narrower than the frequency spacing of the longitudinal laser modes.

With Bragg-gratings of 352-nm and 346-nm-periodicity DBR-lasers for $\lambda_s = 1561$ nm and $\lambda_s = 1531$-nm emission wavelengths have been developed in $\hat{Z}$-cut LiNbO$_3$ [34]. It was even possible to fabricate two lasers of both periods on a common substrate. The gratings have been holographically defined in a resist layer and subsequently transferred into the waveguide surface by sophisticated masking and dry etching techniques [35]. The depth of grooves was limited by redeposition effects during etching to about 420 nm. The upper inset of Fig. 13 shows a SEM top view of a grating of 352-nm periodicity etched 300-nm deep into the surface of LiNbO$_3$.

In Fig. 13, also the power characteristics (a) and the highly resolved spectrum (b) of one of the 1561-nm lasers are shown. The laser has been been fiber-pigtailed, packaged and temperature-stabilized. Diode-pumping at $\lambda_p \simeq 1480$ nm in TE-polarization has been used. At about 45-mW pump power laser oscillation sets in; with 110 mW about 1.4 mW output power has been measured. This poor efficiency is a consequence of the not yet optimized laser cavity with excess losses for pump and signal radiation induced by the grating. Moreover, only single pass pumping is possible with the present design.

The linewidth of the laser emission is very narrow. Using a scanning Fabry–Perot resonator as spectrum analyzer single-frequency operation of the laser could be verified; however, the true linewidth could not be resolved in this way. Therefore, delayed self-heterodyne detection with a 26-km-long fiber as the delay line in one arm of a fiber optical Mach–Zehnder-interferometer has been used for high resolution spectral analysis. An integrated acoustooptical filter was inserted into
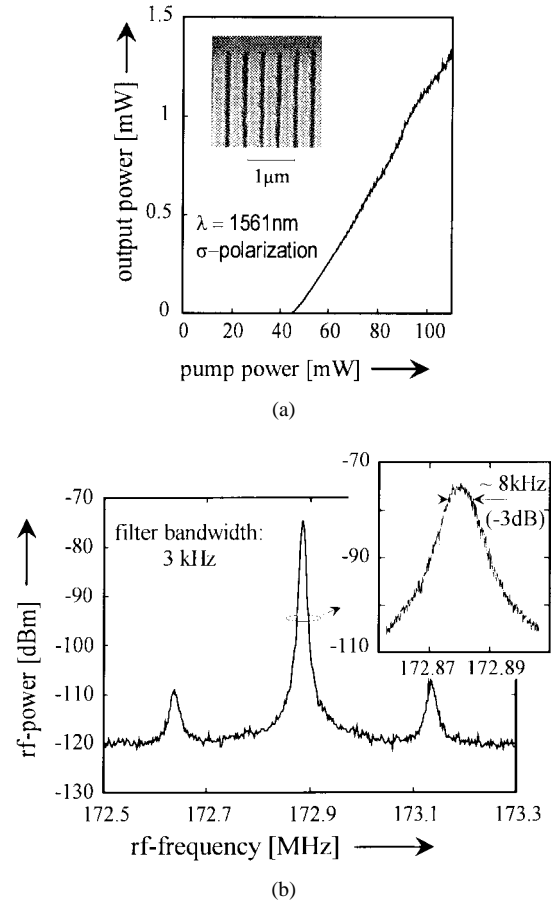

(a)

(b)

Fig. 13. Power characteristics (a) and self-heterodyne beat spectrum (b) of the emission of a diode pumped, pigtailed and packaged single frequency DBR-Ti:Er:LiNbO$_3$-waveguide laser. Upper inset: SEM-image of the dry-etched first-order surface relief grating used as Bragg reflector. Lower inset: Peak of the beat spectrum with higher resolution.

the other arm of the interferometer as frequency shifter. The interferometer output was measured and the resulting electronic beat spectrum is shown in the lower part of Fig. 13. From the 3-dB bandwidth of the spectral power density, the laser linewidth can be determined; it is narrower than 8 kHz. Feedback controlled pumping and a good optical isolation of the laser output were absolutely necessary to achieve this result.

VI. INTEGRATED OPTICAL CIRCUITS

DBR-lasers as presented in Section V-E are key components to develop optically powered monolithic integrated optics in LiNbO$_3$. Circuits of higher functionality and complexity can be designed by combining lasers and further active and passive devices on the same substrate. This new field is of growing interest and open for many ideas to be realized.

As a first example, an integrated transmitter unit has been recently demonstrated consisting of a narrow linewidth DBR-laser and a Mach–Zehnder-type encoding modulator on the same Er-doped substrate [36]. This is a very attractive combination for long-haul fiber optical communication as the extracavity electrooptical waveguide modulator introduces only a negligible wavelength chirp of the laser emission.
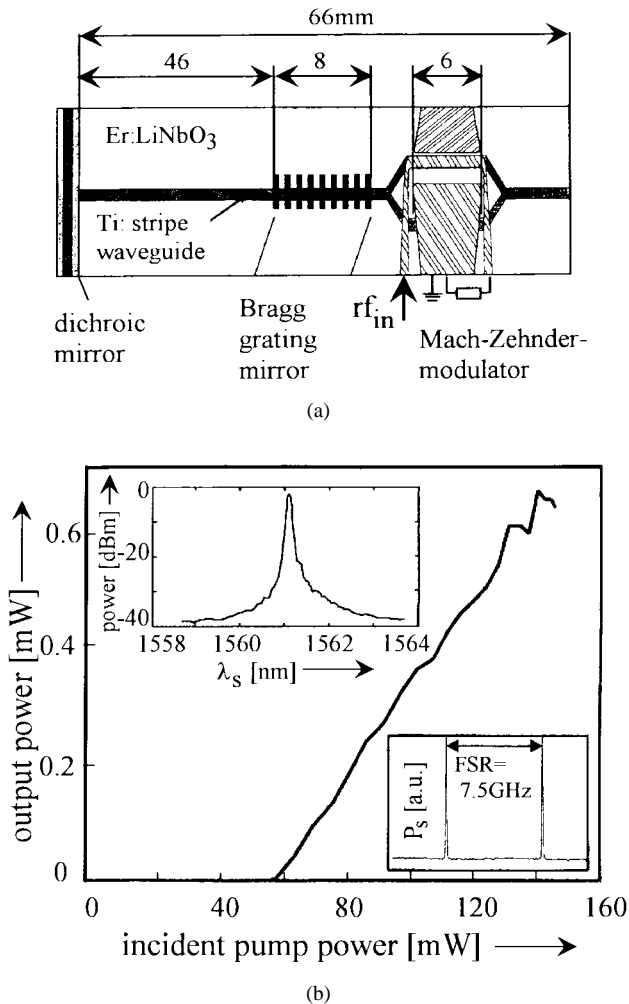
Fig. 14. Structure (schematical) and properties (CW-power characteristics and spectrum (insets)) of an integrated Ti:Er:LiNbO$_3$ DBR-laser-modulator unit (see also text).

The structure of the integrated laser/modulator-unit is sketched schematically in Fig. 14(a); it has been fabricated by 3-in full-wafer technology. The $\hat{Z}$-cut LiNbO$_3$-substrate has been Er-doped over the full transmitter length of 66 mm by indiffusion of a sputtered Er-layer during 100 h at 1100 °C. The laser cavity is comprised of a 8-mm-long first-order (λ_B = 1561 nm) Bragg grating of 352.5-nm period dry etched 300-nm deep into the waveguide surface and a dichroic dielectric mirror at the pump input side. This mirror has a transmittivity of 60% at the pump wavelength ($\lambda_p \simeq$ 1480 nm) and a high reflectivity at the laser emission wavelength (λ_s = 1561 nm). For the grating mirror a transmission drop at the Bragg wavelength > 3.5 dB has been measured for TE-polarized light corresponding to a peak reflectivity >50%. The gain section between the mirrors is 46-mm long. Pump power not absorbed in this section is utilized to provide loss compensation of the DBR-laser signal in the subsequent extracavity Mach–Zehnder-type encoding modulator, which is also Er-doped.

In Fig. 14(b), the measured laser performance is summarized. The laser has a threshold of 54.8-mW incident pump

power. At a pump power level of 145 mW, up to 0.63-mW output power have been measured at the modulator output. The laser emission wavelength is determined by the Bragg wavelength of the grating reflector as shown in the upper left inset of Fig. 14(b). Stable single longitudinal mode operation has been confirmed using a scanning Fabry–Perot interferometer of 7.5-GHz free-spectral range and 37.5-MHz resolution (see lower right inset).

The encoding modulator has traveling-wave Au-electrodes of 6 mm in length and 10 Ω of serial resistance. An insulating SiO$_2$-buffer layer was deposited prior to the electrode fabrication to minimize excess losses in the modulator. Due to the TE-polarized laser emission only the smaller r_{31}-electrooptic coefficient of LiNbO$_3$ could be utilized resulting in a fairly high halfwave voltage V$_\pi$ > 20 V. As a result of this high drive voltage the modulator could only be operated in a lumped electrode configuration. The frequency response of the integrated laser/modulator unit under electrooptic modulation has been measured using an electrooptic spectrum analyzer. A 3 dB optical bandwidth of $\simeq$3 GHz has been achieved.

A significant improvement of the integrated optical transmitter unit will be possible by using $\hat{X}$-cut substrates with Bragg-gratings of high reflectivity for TE-modes. This configuration would allow to utilize the largest electrooptic coefficient r_{33} for the modulation and, thus, permit the application of traveling-wave configurations of very high bandwidth. Moreover, the use of 4-in diameter LiNbO$_3$-wafers would allow the fabrication of longer modulators of a significantly reduced V$_\pi$.

VII. CONCLUSION

Erbium-diffusion-doping of LiNbO$_3$ allows to develop a variety of attractive integrated optical devices. Besides optically pumped waveguide amplifiers and relatively simple Fabry–Perot-type waveguide lasers more advanced devices can be designed by combining optical amplification and/or lasing with electro- or acoustooptically controlled functions in the same waveguide (laser) structure. Examples are amplifying electrooptical phase- and intensity modulators, high finesse Fabry–Perot-type optical spectrum analyzers and tunable, acoustooptical, polarization-dependent and -independent wavelength filters. Furthermore, modelocked, Q-switched and tunable lasers have been developed in this way. Additional functions can be expected by combining optical amplification with different nonlinear effects. All-optical switching bistable behavior and parametric frequency conversion might be achieved in well-designed erbium-doped structures.

Moreover, Er-doped DBR-lasers can be easily combined with additional active and passive devices on the same substrate to form optical circuits of higher functionality. Laser–modulator combinations are the first examples. More sophisticated circuits will be heterodyne interferometers for optical metrology and vibration analysis with a DBR-laser and up to 11 additional devices [37]. It is a challenge for the future to design and to develop complex, optically powered, monolithic integrated optics in (selectively) Er-doped LiNbO$_3$ with new application specific optical circuits.

REFERENCES

[1] E. Lallier, J. P. Pocholle, M. Papuchon, C. Grezes-Besset, E. Pelletier, M. De Micheli, M. J. Li, Q. He, and D. B. Ostrowsky, "Laser oscillation of single mode channel waveguide in Nd:MgO:LiNbO$_3$," *Electron. Lett.,* vol. 25, no. 22, pp. 1491–1492, 1989.

[2] R. Brinkmann, W. Sohler, H. Suche, and Ch. Wersig, "Single mode Ti-diffused optical strip guides and lasers in Nd:MgO:LiNbO$_3$," in *Tech. Dig. Integrated Photonics Research.* Washington, DC: Opt. Soc. Amer., 1990, vol. 5, pp. 116–117.

[3] E. Lallier, J. P. Pocholle, M. Papuchon, Q. He, M. De Micheli, D. B. Ostrowsky, C. Grezes-Besset, E. Pelletier, "Integrated Nd:MgO:LiNbO$_3$ FM mode-locked waveguide laser," *Electron. Lett.*, vol. 27, no. 11, pp. 936–937, 1991.

[4] E. Lallier, D. Papillon, J. P. Pocholle, M. Papuchon, M. De Micheli, D. B. Ostrowsky, "Short pulse, high power Q-switched Nd:MgO:LiNbO$_3$ waveguide laser," *Electron. Lett.,* vol. 29, no. 2, pp. 175–176, 1993.

[5] J. Amin, M. Hempsted, J. E. Román, and J. S. Wilkinson, "Tunable coupled-cavity waveguide laser at room temperature in Nd-diffused Ti:LiNbO$_3$," *Opt. Lett.* vol. 19, no. 19, pp. 1541–1543, 1994.

[6] J. P. de Sandro, J. K. Jones, D. P. Shepherd, J. Webjörn, M. Hempstead, J. Wang, and A. C. Tropper, "Tm^{3+} indiffused LiNbO$_3$ waveguide lasers," in *Proc. 7th Eur. Conf. Integrated Optics (ECIO '95)*, Delft, The Netherlands, 1995, pp. 17–20, post-deadline papers.

[7] J. K. Jones, J. P. De Sandro, M. Hempstead, D. P. Shepherd, A. C. Large, A. C. Tropper and J. S. Wilkinson, "Channel waveguide laser at 1 μm in Yb-indiffused LiNbO$_3$," *Opt. Lett.* vol. 20, no. 13, pp. 1477–1479, 1995.

[8] W. Sohler, "Erbium-Doped Waveguide Amplifiers and Lasers in LiNbO$_3$," in *Tech. Dig. Integrated Photonic Research, OSA Tech. Dig. Series.* Washington, DC: Opt. Soc. Amer., 1995, vol. 7, pp. 212–214, (invited) and references cited therein.

[9] H. Suche, D. Hiller, I. Baumann, and W. Sohler, "Integrated Optical Spectrum Analyzer with Internal Gain," *IEEE Photon. Technol. Lett.*, vol. 7, pp. 505–507, May 1995.

[10] R. Brinkmann, M. Dinand, I. Baumann, Ch. Harizi, W. Sohler, and H. Suche, "Acoustically tunable wavelength filter with gain," *Phot. Technol. Lett.*, vol. 6, pp. 519–521, Apr. 1994)

[11] I. Baumann, R. Brinkmann, M. Dinand, W. Sohler and S. Westenhöfer, "Ti:Er:LiNbO$_3$ waveguide laser of optimized efficiency," *IEEE J. Quantum Electron.*, vol. 32, pp. 1695–1706, Sept. 1996.

[12] H. Suche, I. Baumann, D.Hiller, and W. Sohler, "Modelocked Er:Ti:LiNbO$_3$-Waveguide Laser," *Electron. Lett.*, vol. 29, no. 12, pp. 1111–1112, 1993.

[13] H. Suche, R. Wessel, S. Westenhöfer, W. Sohler, S. Bosso, C. Carmannini, and R. Corsini,, "Harmonically modelocked Ti:Er:LiNbO$_3$-waveguide laser," *Opt. Lett.* vol. 20, no. 6, pp. 596–598, 1995.

[14] I. Baumann, D. Johlen, W. Sohler, H. Suche, and F. Tian, "Acoustically tunable Ti:Er:LiNbO$_3$-waveguide laser," in *Proc. 20th Eur. Conf. Optical Communication (ECOC '94),* Florence, Italy, 1994, vol. 4, pp. 99–102, post deadline papers.

[15] W. Sohler, "Integrated optical circuits with ErLiNbO$_3$ amplifiers and lasers," *Optical Fiber Communication Conf., vol. 2, 1996 OSA Tech. Dig. Ser.* Washington, DC: Opt. Soc. Amer., 1996, pp. 251, invited paper.

[16] L. F. Johnson and A. A. Ballman, "Coherent Emission from Rare Earth Ions in Electro-optic Crystals," *J. Appl. Phys.*, vol. 40, no. 1, pp. 297–302, 1969.

[17] N. F. Evlanova and L. N. Rashkovich, "Domain structure of lithium metaniobate crystals," *Sov. Solid State Phys.*, vol. 13, no. 1, pp. 223–224, 1971.

[18] R. Brinkmann, Ch. Buchal, St. Mohr, W. Sohler, and H. Suche, "Annealed erbium-implanted single-mode LiNbO$_3$ waveguides," in *Tech. Dig. Integrated Photonics Research.* Washington, DC: Opt. Soc. Amer., 1990, vol. 5, post-deadline paper PD1.

[19] W. Sohler and H. Suche, "Rare-earth-doped lithium niobate waveguide structures," Eur. Patent No. 0 569 353 and U. S. Patent Application Serial No. 08 094 199

[20] I. Baumann, R. Brinkmann, Ch. Buchal, M. Dinand, M. Fleuster, H. Holzbrecher, W. Sohler, and H. Suche, "Er-diffused Waveguides in LiNbO$_3$," in *Proc. Eur. Conf. Integrated Optics, ECIO'93*, Neuchâtel, 1993, paper 3-14.

[21] I. Baumann, L. Beckers, Ch. Buchal, R. Brinkmann, M. Dinand, Th. Gog, H. Holzbrecher, M. Fleuster, M. Materlik, K. H. Müller, H. Paulus, W. Sohler, H. Stolz, W. von der Osten, O. Witte, "Erbium incorporation in LiNbO$_3$ by diffusion-doping," *Appl. Phys. A*, to be published.

[22] T. Gog, M. Griebenow, and G. Materlik, "X-ray standing wave determination of the lattice location of Er diffused into LiNbO$_3$," *Phys. Lett. A*, vol. 181, no. 5, pp. 417–420, 1993.

[23] O. Witte, H. Stolz, and W. von der Osten, "Upconversion and site-selective spectroscopy in erbium-doped LiNbO$_3$," *J. Phys. D, Apppl. Phys.*, vol. 29, pp. 561–568, 1996.

[24] P. F. Bordui, R. G. Norwood, C. D. Bird, and G. D. Calvert, "Compositional uniformity in growth and poling of large-diameter lithium niobate crystals," *J. Crystal Growth*, vol. 113, pp. 61–68, 1991.

[25] R. Brinkmann, I. Baumann, M. Dinand, W. Sohler, and H. Suche, "Erbium-doped single- and double-pass Ti,LiNbO$_3$ waveguide amplifiers," *IEEE J. Quantum Electron.*, vol. 30, pp. 2356–2360, Oct. 1994.

[26] H. Okamura and K. Iwatsuki, "A Finesse-Enhanced Er-Doped-Fiber Ring Resonator," *IEEE J. Quantum Electron.* vol. QE-29, pp. 1554–1560, Nov. 1991.

[27] K. Hattori, "Planar silica waveguide amplifiers and related circuits," *Tech. Dig. 5th Optoelectronics Conf., OEC'94*, Chiba, Japan, 1994, pp. 162–163.

[28] K. W. Cheung, S. C. Liew, C. N. Lo, D. A. Smith, J. E. Baran, and J. J. Johnson, "Simultaneous five-wavelength filtering at 2.2 nm separation using acoustooptic tunable filter with subcarrier detection," *Electron. Lett.*, vol. 25, pp. 636–637, 1989.

[29] H. Herrmann, P. Müller-Reich, R. Reimann, R. Ricken, H. Seibert, and W. Sohler, "Integrated optical, TE- and TM-pass acoustically tunable, double-stage wavelength filters in LiNbO$_3$," *Electron. Lett.*, vol. 28, no. 7, pp. 642–643, 1992.

[30] R. Brinkmann, W. Sohler and H. Suche, "Continuous-Wave Erbium-Diffused LiNbO$_3$ Waveguide-Laser," *Electron. Lett.*, vol. 27, no. 5, pp. 415–416, 1991.

[31] P. Becker, R. Brinkmann, M. Dinand, W. Sohler, and H. Suche, "Er-diffused Ti:LiNbO$_3$ waveguide laser of 1563 and 1576 nm emission wavelengths," *Appl. Phys. Lett.*, vol. 61, no. 11, pp. 1257–1259, 1992.

[32] M. Dinand and W. Sohler, "Theoretical modeling of optical amplification in Er-doped Ti:LiNbO$_3$ waveguides," *J. Quantum Electron.*, vol. 30, pp. 1267–76, May 1994.

[33] D. J. Kuizenga and A. E. Siegman, "FM and AM Mode Locking of the Homogeneous Laser—Part I, Theory," *IEEE J. Quantum Electron.*, vol. 6, pp. 694–708, 1970.

[34] J. Söchtig, R. Gross, I. Baumann, W. Sohler, H. Schütz, and R. Widmer, "DBR waveguide laser in erbium-diffusion-doped LiNbO$_3$," *Electron. Lett.*, vol. 31, no. 7, pp. 551–552, 1995.

[35] J. Söchtig, H. Schütz, R. Widmer, R. Lehmann, and R. Gross, "Grating reflectorsfor erbium-doped lithium niobate waveguide lasers," *Proc. SPIE Conf., Nanofabrication and Device Integration*, vol. 2213, 1994, pp. 98–107.

[36] J. Söchtig, H. Schütz, R. Widmer, R. Corsini, D. Hiller, C. Carmannini, G. Consonni, S. Bosso, and L. Gobbi, "Monolithically integrated DBR waveguide laser and intensity modulator in erbium doped LiNbO$_3$," *Electron. Lett.*, vol. 32, no. 10, pp. 899–900, 1996.

[37] F. Tian, R. Ricken, S. Schmid, and W. Sohler, "Integrated Acousto-optical heterodyne interferometer in LiNbO$_3$," in *Laser in der Technik, Proc. Congr. Laser '93*, Munich, Germany, W. Waidlich, Ed. Berlin, Germany: Springer Verlag, 1993, pp. 725–728.

[38] EU-project "EDIOLL," unpublished investigations.

I. Baumann, photograph and biography not available at the time of publication.

S. Bosso, photograph and biography not available at the time of publication.

R. Brinkmann, photograph and biography not available at the time of publication.

R. Corsini, photograph and biography not available at the time of publication.

M. Dinand, photograph and biography not available at the time of publication.

A. Greiner, photograph and biography not available at the time of publication.

K. Schäfer, photograph and biography not available at the time of publication.

J. Söchtig, photograph and biography not available at the time of publication.

W. Sohler, photograph and biography not available at the time of publication.

H. Suche, photograph and biography not available at the time of publication.

R. Wessel, photograph and biography not available at the time of publication.